JACS
JOURNAL OF THE AMERICAN CHEMICAL SOCIETY
Article
pubs.acs.org/JACS

Unraveling the Mechanisms of O_2 Activation by Size-Selected Gold Clusters: Transition from Superoxo to Peroxo Chemisorption

Rhitankar Pal,[†] Lei-Ming Wang,[‡] Yong Pei,[§] Lai-Sheng Wang,*[,∥] and Xiao Cheng Zeng*[,†]

[†]Department of Chemistry, University of Nebraska-Lincoln, Lincoln, Nebraska, 68588, United States
[‡]Department of Physics and Astronomy, University of Pittsburgh, Pittsburgh, Pennsylvania 15260, United States
[§]Department of Chemistry, Key Laboratory of Environmentally Friendly Chemistry and Applications of Ministry of Education, Xiangtan University, Hunan Province, China 411105
[∥]Department of Chemistry, Brown University, Providence, Rhode Island 02912, United States

Supporting Information

ABSTRACT: The activation of dioxygen is a key step in CO oxidation catalyzed by gold nanoparticles. It is known that small gold cluster anions with even-numbered atoms can molecularly chemisorb O_2 via one-electron transfer from Au_n^- to O_2, whereas clusters with odd-numbered atoms are inert toward O_2. Here we report spectroscopic evidence of two modes of O_2 activation by the small even-sized Au_n^- clusters: superoxo and peroxo chemisorption. Photoelectron spectroscopy of $O_2Au_8^-$ revealed two distinct isomers, which can be converted from one to the other depending on the reaction time. Ab initio calculations show that there are two close-lying molecular O_2-chemisorbed isomers for $O_2Au_8^-$: the lower energy isomer involves a peroxo-type binding of O_2 onto Au_8^-, while the superoxo chemisorption is a slightly higher energy isomer. The computed detachment transitions of the superoxo and peroxo species are in good agreement with the experimental observation. The current work shows that there is a superoxo to peroxo chemisorption transition of O_2 on gold clusters at Au_8^-: $O_2Au_n^-$ (n = 2, 4, 6) involves superoxo binding and n = 10, 12, 14, 18 involves peroxo binding, whereas the superoxo binding re-emerges at n = 20 due to the high symmetry tetrahedral structure of Au_{20}, which has a very low electron affinity. Hence, the two-dimensional (2D) Au_8^- is the smallest anionic gold nanoparticle that prefers peroxo binding with O_2. At Au_{12}^-, although both 2D and 3D isomers coexist in the cluster beam, the 3D isomer prefers the peroxo binding with O_2.

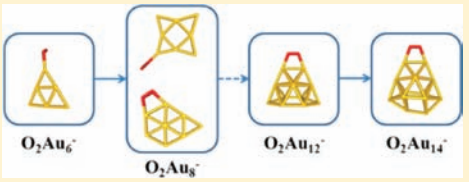

INTRODUCTION

Although bulk gold has long been known to be the most chemically inert metal, nanosized gold particles have demonstrated unusual capability in catalyzing a wide variety of chemical reactions, e.g. CO oxidation,[1] epoxidation,[2,3] selective hydrogenation/reduction,[4] C−C bond formation,[5] and water−gas shift.[6] Especially, the CO oxidation reaction catalyzed by supported gold nanostructures has attracted considerable attention.[1,7−17] However, despite intensive investigations, the exact mechanisms for the CO oxidation by gold are still not well understood, in part, due to the lack of precise experimental characterization of the O_2 activation, a key step in gold nanocatalysis.

Early reactivity studies of Au_n^- toward O_2 revealed molecular O_2 addition as the main reaction channel for the even-sized clusters, whereas the odd-sized clusters are inert toward O_2.[18−20] The even−odd alternation correlates well with a similar trend in the electron affinities of Au_n suggesting that electron transfer from Au_n^- to O_2 might be the primary reaction and activation mechanism.[20] In subsequent photoelectron spectroscopy (PES) studies,[21,22] experimental evidence was reported, showing that the even-sized $Au_nO_2^-$ clusters are indeed molecularly chemisorbed complexes via the observation of O−O vibrational structures. Recent PES experiment from our lab has confirmed the molecular chemisorption of O_2 on Au_n^- for n = 2, 4, 6 and further provided evidence that O_2 physisorbed onto Au_n^- for n = 3, 5, 7.[23] Among the small even-sized clusters, the O_2 reactivity of Au_{10}^- and Au_{16}^- was unusual: Au_{16}^- was found to be unreactive with O_2, while Au_{10}^- was significantly less reactive.[20] We have recently found that the inertness of Au_{16}^- is due to its unique cage structures[24] and its high electron binding energy because the corresponding neutral Au_{16} cage possesses a triplet ground state. For Au_{10}^-, we found recently that the global minimum D_{3h} isomer is unreactive with O_2, whereas only the weakly populated low-lying isomers are reactive.[25]

The binding of O_2 on unsupported gold clusters has been studied computationally.[26−34] Yoon et al. first reported that small Au_n (n = 2−8) clusters can molecularly chemisorb O_2 for n = 2 and 3, regardless of the charge states, but they found that dissociative adsorption is favored thermodynamically for $n \geq 4$.[26] However, the activation energies for O_2 dissociation are found to be more than 2 eV for n = 5 and 6. Such high barriers seemed to be consistent with the experimental observation of only molecular O_2 chemisorption on even-sized Au_n^- clusters

Received: March 25, 2012
Published: May 9, 2012

dx.doi.org/10.1021/ja302902p | J. Am. Chem. Soc. 2012, 134, 9438−9445

for $n \leq 20$.[18−22] as well as physisorbed odd-sized Au_n^- for n = 3, 5, 7.[23] The spectroscopic signature of molecular O_2 chemisorption on even-sized Au_n^- clusters came from low binding energy detachment features from superoxide-like O_2^- in the PES spectra.[21−23] Clear O−O vibrational structures were observed for n = 2, 4, 6 in these low binding energy O_2-induced detachment features. Similar low binding energy O_2-induced features were also observed for n = 8 and 20, albeit not vibrationally resolved (ref 22; also see Figure 1 for better

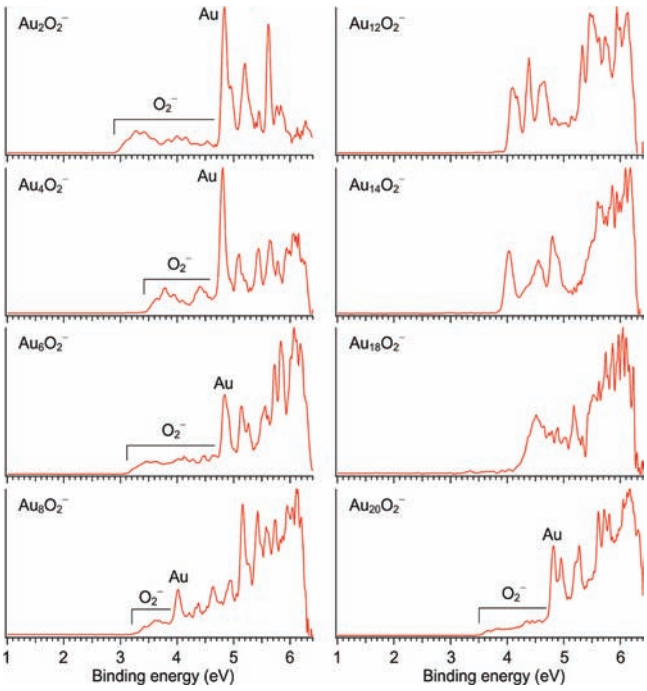

Figure 1. Comparison of the 193 nm photoelectron spectra of $Au_nO_2^-$ (n = 2, 4, 6, 8, 12, 14, 18, 20). The superoxo-derived features are labeled for n = 2, 4, 6, 8, 20. The data for n = 2, 4, 6 are from ref 23.

resolved PES spectra from the current study). However, one puzzling observation was that similar O_2-derived low binding energy features were not observed for n = 12, 14, 18 (Figure 1). The question is: what is the nature of O_2 chemisorption on these even-sized clusters? Resolving this question would bring deeper insights into how O_2 activation is affected by structure, size, and electronic properties of the underlying gold nanostructures.

Here we report a detailed PES and theoretical study of O_2 chemisorption on even-sized Au_n^- clusters and provide spectroscopic and electronic evidence of the transition from superoxo to peroxo chemisorption at Au_8^-. The superoxo form involves a single O−Au bond (η^1-O_2), whereas the peroxo form involves two O−Au bonds (η^2-O_2). Both forms are observed to coexist in the cluster beam of $O_2Au_8^-$. The superoxo $O_2Au_8^-$ gives rise to low binding energy O_2-induced PES features, similar to those observed for n = 2, 4, 6, and 20, whereas the peroxo $O_2Au_8^-$ gives rise to sharper higher binding energy features similar to those observed for n = 12, 14, 18 (Figure 1). The superoxo $O_2Au_8^-$ is observed to convert to the peroxo form under longer reaction time using a newly designed cluster reactor. Detailed theoretical calculations have been carried out and confirmed the experimental observations. Although the dissociative $O_2Au_8^-$ is the most stable form, the barrier for O_2 dissociation is too high (>2 eV) for it to be observed experimentally. The peroxo $O_2Au_8^-$ is shown to be the next low-lying isomer, followed by the superoxo form. The simulated detachment spectra of the two molecularly chemisorbed $O_2Au_8^-$ isomers are in good agreement with the experiment, confirming the transition from superoxo to peroxo chemisorption at Au_8^-. In addition, we find that although both two-dimensional (2D) and 3D isomers of Au_{12}^- coexist in the cluster beam, O_2 prefers the peroxo binding with the 3D isomer.

EXPERIMENTAL METHODS

The PES experiment was carried out using a magnetic-bottle type apparatus equipped with a laser vaporization supersonic cluster source, details of which have been described elsewhere.[35] In the current study, the reactions of O_2 with gold clusters were performed in two different methods. In the first method, the $O_2Au_8^-$ complexes were generated by laser vaporization of a pure gold target in the presence of a He carrier gas seeded with 0.1% O_2. This method was used previously to produce smaller molecularly chemisorbed $O_2Au_n^-$ complexes.[23] In the second method, $O_2Au_8^-$ complexes were produced using a flow-tube reactor, which consisted of a 30-mm long stainless tube with an inner diameter of 6 mm and either an open end or a 3-mm outlet orifice. The flow-tube reactor was attached to the cluster nozzle, and the O_2 reactant was introduced into the reaction tube after the gold clusters were formed. The large volume of the flow reactor allowed more reaction times and adequate thermalization of the clusters. Negatively charged clusters were analyzed by a time-of-flight mass spectrometer. The clusters of interest were selected and decelerated before photodetachment in the interaction zone of the magnetic-bottle electron analyzer. PES spectra of $O_2Au_n^-$ were measured at 193 nm (6.424 eV) from an ArF excimer laser. The PES spectrometer was calibrated using the known spectrum of Au^-. The resolution of the PES apparatus ($\Delta E/E$) was about 2.5%, i.e. 25 meV for 1 eV electrons.

COMPUTATIONAL METHODS

The theoretical study employed the basin-hopping (BH) global search method[36,37] coupled with density-functional theory (DFT) optimization to search for low-lying isomers of $O_2Au_8^-$. Generalized gradient approximation (GGA) in the Perdew−Burke−Ernzerhof (PBE) functional form was used for the DFT calculations. Multiple initial structures were used as the input for the BH search. After more than 500 BH steps, a consistent set of low-lying isomers were generated for each species. Several low-lying isomers (typically within 1.0 eV of the lowest-energy isomer) were used to compute the electronic density of states (DOS). These low-lying structures were reoptimized at the PBE0/CRENBL level of theory implemented in the *NWChem* 5.1 package.[38] Single-point energy calculations at the PBE0/CRENBL level with the inclusion of spin−orbit (SO) effects were then used to obtain the computed density of states. The inclusion of the SO effects was previously shown to yield almost quantitative agreement between the experimental photoelectron spectra and computed DOS for gold clusters.[39−42] The first VDE of each isomer was calculated as the difference between the energy of the anionic species of each isomer and the corresponding neutral at the anion geometry. The spin states of these neutral species are crucial, and the energy of the lowest spin state was used to compute the first VDE. The binding energies of the deeper occupied orbitals of the anion were then added to the first VDE to approximate higher binding energy PES features. Each computed VDE was fitted with a Gaussian of 0.06 eV width to yield a computed photoelectron spectrum, which was used to compare with spectra of the experimental data.

RESULTS AND DISCUSSION

The 193 nm PES spectra of $O_2Au_n^-$, produced using the O_2-seeded He carrier gas, are presented in Figure 1 for all the even-sized species for n = 2, 4, 6, 8, 12, 14, 18, 20. These spectra are consistent with those reported previously,[22] but with slightly

dx.doi.org/10.1021/ja302902p | J. Am. Chem. Soc. 2012, 134, 9438−9445

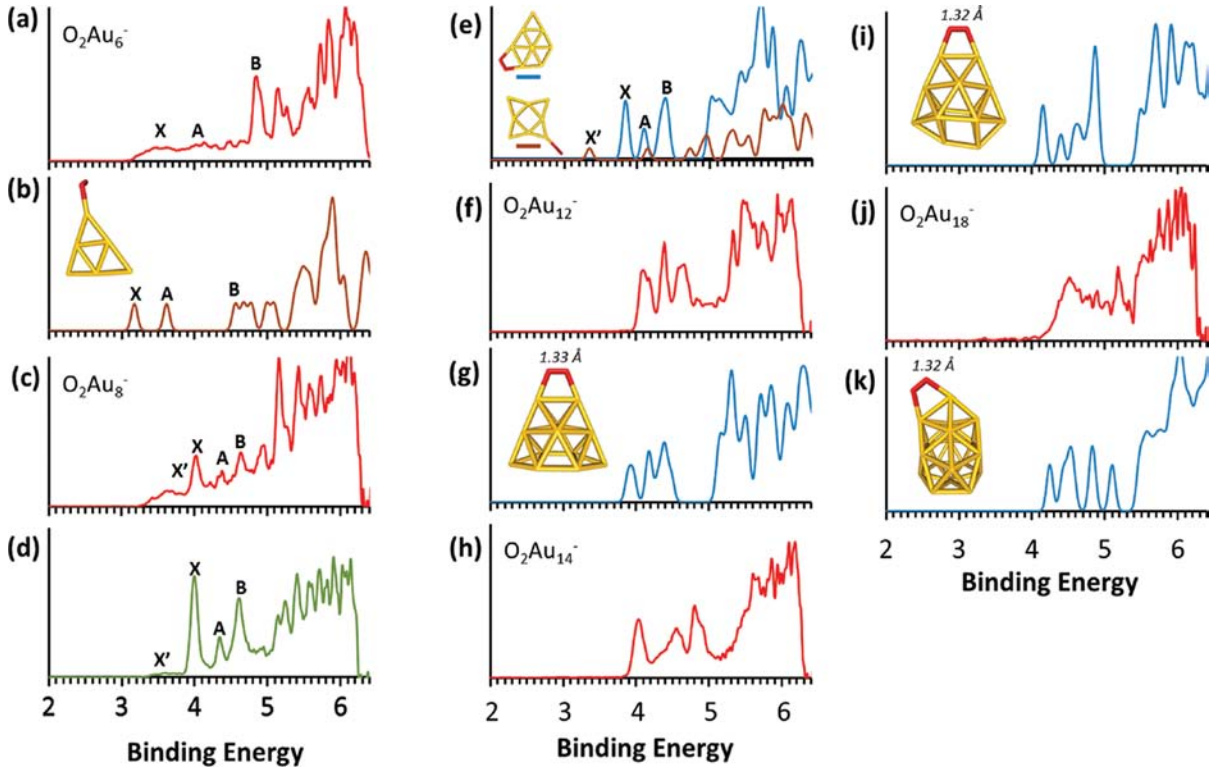

Figure 2. Comparison of the experimental PES spectra of $O_2Au_6^-$ (a), $O_2Au_8^-$ (c and d), $O_2Au_{12}^-$ (f), $O_2Au_{14}^-$ (h), and $O_2Au_{18}^-$ (j)] with the computed spectra and the corresponding structures [(b), (e), (g), (i), (k)]. The experimental spectra of $O_2Au_8^-$ (c and d) were obtained under two different experimental conditions (see text). The simulated spectra of the superoxo and peroxo isomers are represented in brown and blue colors, respectively.

improved resolution. The weak and broad spectral features in the low binding energy side in the spectra of n = 2, 4, 6, 8, 20 are indicative of the unresolved O−O vibrational progressions upon photodetachment from an O_2^- superoxide unit.[22,23] The same spectra were obtained using the flow reactor for all the species except for $O_2Au_8^-$, as shown in Figure 2c and d.

In the flow reactor, the O_2 reactant was introduced after the gold clusters were formed. Furthermore, we could control the reaction time to some degree by using a different orifice at the exit of the flow reactor. When a reactor tube with an open end was used, corresponding to a short reaction time, we obtained a PES spectrum of $O_2Au_8^-$ (Figure 2c) similar to that shown in Figure 1. However, when we used a reactor tube with a 3-mm diameter exit orifice, we obtained the PES spectrum displayed in Figure 2d, in which the low binding energy feature (X′) was almost completely eliminated, due to the increased reaction time in the flow reactor. This observation suggested the initially formed superoxo species were converted to a new isomer, which gave rise to three relatively sharp PES bands (X, A, and B) between 4 and 5 eV (Figure 2d). A close examination shows that the three corresponding peaks are also present in the spectrum in Figure 2c, suggesting that both isomers coexisted. However, we did not observe any spectral changes for smaller even-sized $O_2Au_n^-$ complexes using the flow reactor. Figure 2a displays a 193 nm spectrum of $O_2Au_6^-$ using the reactor with the 3-nm diameter exit. This spectrum is identical to the one taken using the O_2-seeded He carrier gas, reported previously,[23] suggesting that the even-sized $O_2Au_n^-$ complexes with n < 8 contain only the superoxo chemisorption form.

$O_2Au_6^-$. The previous theoretical study on $O_2Au_6^-$ showed that the dissociative chemisorption is the global minimum with a large barrier for O_2 dissociation[26] and thus is not expected to be accessible experimentally. The closest low-lying isomer corresponds to O_2 bonded to an apex gold atom in the triangular Au_6 in the superoxo form (Figure 2b). To compare with $O_2Au_8^-$, we recalculated the top four isomers of $O_2Au_6^-$ at the SO-PBE0/CRENBL level of theory: the simulated PES spectra with SO coupling along with their relative energies are shown in Figure S1, Supporting Information [SI]. The neutral of each isomer can exist in either spin triplet (S = 3; here S denotes spin multiplicity) or spin singlet (S = 1). The energies of both spin states were examined, and the triplet states were found to be more stable for all the isomers, (a)−(d), shown in Figure S1, SI. We also found that the dissociated isomer (a) is the global minimum, but the high activation barrier from the molecular to dissociated form makes it inaccessible under our experimental conditions. The resolved O−O vibrational structures for the low binding energy features at 266 nm[23] firmly ruled out the presence of the dissociated form of $O_2Au_6^-$.

The lowest molecularly chemisorbed species is the superoxo isomer (b) (Figure 2b and Figure S1b, SI). Both the calculated first few VDEs (Table 1) and the simulated spectrum (Figure

Table 1. Experimental VDEs Compared with the Calculated Values for the Lowest-Energy Molecularly Chemisorbed Superoxo Isomer of $O_2Au_6^-$ Using NWChem 5.1 at the Level of SO-PBE0/CRENBL

VDE	expt	SO-DFT
X	~3.4	3.14
A	~4.0	3.58
B	4.84 ± 0.04	4.53

dx.doi.org/10.1021/ja302902p | J. Am. Chem. Soc. 2012, 134, 9438−9445

2b) are in good agreement with the experimental data. As reported in our previous studies,[39−43] the VDEs calculated with SO−DFT are usually too low by ∼0.2−0.4 eV relative to the experimental data, as is also the case for $O_2Au_6^-$ (Table 1). As shown in Figure 3a,b, the HOMO and HOMO−1 of the

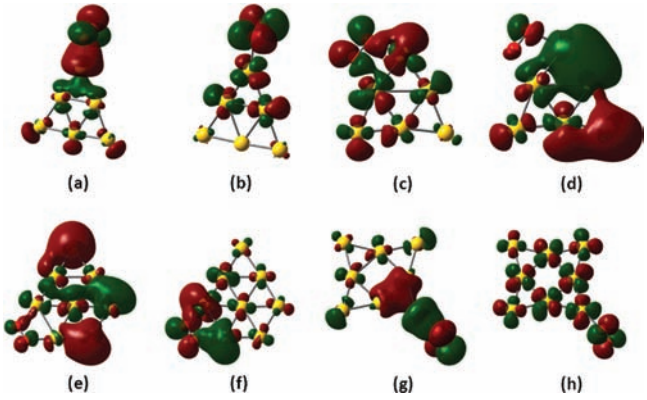

Figure 3. HOMO and HOMO−1 of the superoxo [(a) and (b)] and peroxo [(c) and (d)] isomer of $O_2Au_6^-$; and that of peroxo [(e) and (f)] and superoxo [(g) and (h)] isomer of $O_2Au_8^-$.

superoxo $O_2Au_6^-$ are essentially the π^* orbitals on the superoxo unit, in agreement with the observed O−O vibrations in the X and A bands.[23] The next higher lying isomer of $O_2Au_6^-$ is the peroxo isomer [Figure S1c (SI)]. Both the experimental observation and the theoretical calculations can rule out the existence of this isomer.

$O_2Au_8^-$. Our basin-hopping search combined with DFT optimization generated about 500 structures for $O_2Au_8^-$, consisting of both molecularly chemisorbed and dissociated isomers. The top candidate structures within 1.0 eV from the lowest-lying isomer were reevaluated using SO-PBE0/CRENBL calculations and the computed photoelectron spectra along with relative energies are presented in Figure S2 (SI). The global minimum of $O_2Au_8^-$ is the dissociated structure [Figure S2a (SI)], similar to that reported previously.[26] The second low-lying isomer is the molecularly chemisorbed peroxo form, which is 0.355 eV higher in energy at the PBE0/CRENBL level (Table 2). This structure was not reported

Table 2. Relative Energies of the Four Lowest-Lying Isomers (a), (b), (c) and (d) of $O_2Au_8^-$ at SO-PBE0, TPSSh, and CCSD(T) Levels of Theory

isomers	Δ*E* (eV) SO-PBE0/aug-cc-pVTZ (O) /CRENBL ECP (Au)	Δ*E* (eV) TPSSh/6-311+G*(O) /SDD (Au)	Δ*E* (eV) CCSD(T)/6-311+G*(O) /SDD (Au)//SO-PBE0
(a)	0.000	0.000	0.000
(b)	0.355	0.369	1.232
(c)	0.531	0.518	1.480
(d)	0.552	0.151	0.650

before.[26] The next isomer is a superoxo form [Figure S2c (SI)], whereas another dissociative isomer [Figure S2d (SI)] is almost degenerate with the superoxo isomer at the PBE0/CRENBL level (Table 2). The parent gold clusters are different in the two molecularly chemisorbed $O_2Au_8^-$ complexes and they represent the two nearly degenerate lowest energy structures of Au_8^-.[39]

In our previous theoretical study on CO-adsorbed gold clusters,[43] we found that meta-GGA functionals gave more consistent relative energies in comparison with coupled-cluster calculations at the CCSD(T) level. Hence, we have computed the relative energies of the four leading candidates for $O_2Au_8^-$ using the meta-GGA functional (TPSSh) and at the CCSD(T) level, as shown in Table 2. The TPSSh results are in full agreement with the SO-PBE0 energies for the isomers (a)−(c), although the second dissociative isomer (d) is favored relative to the two molecularly chemisorbed species (b and c) at the TPSSh level. At the CCSD(T) level, however, the dissociative isomer (a) was found to be stabilized by a very large energy margin (>1 eV) relative to the two molecularly chemisorbed isomers, but the energy ordering is the same as that at the TPSSh level. Vibrational frequencies calculated for all the isomers from (a)−(l) at the TPSSh level show no imaginary values (Table S1[SI]).

However, dissociative chemisorption of O_2 on unsupported gold clusters has not been observed experimentally. Yoon et al. showed previously using DFT calculations that for $O_2Au_4^-$ the dissociated form is already lower in energy than the molecular chemisorption, but there is a high barrier for O_2 dissociation.[26] Their calculated activation barrier for O_2 on Au_6^- was 2.33 eV, in agreement with the experimental observation that only molecular chemisorption was observed for $O_2Au_6^-$.[23] We also calculated the activation barrier for O_2 dissociation on Au_8^- using isomer (b) as the initial molecular complex. As shown in Figure S3 (SI), we obtained an equally high barrier of 2.35 eV at the level of TPSSh. At MP2 level, an even higher barrier of 4.7 eV was obtained. Such a large barrier suggests that again the dissociative state in $O_2Au_8^-$ is not accessible, similar to that in $O_2Au_6^-$.

The computed PES spectra at the SO-PBE0/CRENBL level of theory for all the isomers (a)−(l) are shown in Figure S2 (SI). The corresponding neutral species can exist in either spin triplet ($S = 3$) or spin singlet ($S = 1$). The energies of both spin states were examined and the triplet states were found again to be more stable for all the isomers. Although the first VDE of the global minimum dissociative isomer (a) agrees with the experimental peak X, the spectral pattern is not in good agreement with the observed spectrum. This observation along with the high barrier ruled out the presence of the dissociative isomer for $O_2Au_8^-$. The simulated spectra for the two low-lying peroxo and superoxo forms of $O_2Au_8^-$ are compared with the experimental spectra in Figure 2e and good agreement between the computed spectra and the experimental PES data (Figure 2c,d) can be clearly seen. The VDEs for these two molecular O_2 isomers are compared with the experimental data in Table 3. At the SO-PBE0/CRENBL level, the first VDE of the peroxo isomer (b) (3.79 eV) is slightly low compared to the experimental value of peak X (4.00 eV). This small discrepancy is consistent with our earlier studies,[43−47] including $O_2Au_6^-$ in the current study. The second and third VDEs of isomer (b)

Table 3. Experimental VDEs Compared with the Calculated Values for the Two Molecularly Chemisorbed Isomers of $O_2Au_8^-$, Using NWChem 5.1 at the Level of SO-PBE0/CRENBL

VDE	expt	SO-DFT (*superoxo*)	SO-DFT(*peroxo*)
X′	∼3.6	3.34	–
X	4.00 ± 0.04	–	3.79
A	4.35 ± 0.05	–	4.06
B	4.63 ± 0.04	–	4.34

dx.doi.org/10.1021/ja302902p | *J. Am. Chem. Soc.* 2012, 134, 9438−9445

are also found to be low relative to the respective experimental features, A and B. However, the simulated spectral pattern for X, A, B is in excellent agreement with the experiment (Figure 2e).

The superoxo isomer (c) yields a relatively low first VDE of 3.34 eV, in good agreement with the weak feature X′ in the experimental spectrum. The X′ feature in the experiment is very broad, likely a result of O−O vibrational excitation upon photodetachment from isomer (c). The higher binding energy PES features from isomer (c) overlapped with those from the more dominating isomer (b) in Figure 2c, and are thus difficult to be resolved.

It should be noted that only the superoxo isomer (c) shows vibrational broadening in the low binding energy peak (X′), similar to those observed in $O_2Au_6^-$ (Figure 2a), whereas the spectral features (e.g., X, A, and B) from the peroxo isomer (b) are relatively sharp (Figure 2d). These observations can be understood from the nature of the HOMO and HOMO−1 for the two molecularly chemisorbed isomers (Figure 3). The HOMO of the superoxo isomer (c) (Figure 3g) consists of essentially a pure π^* orbital on the O_2^- unit, which is expected to result in significant vibrational excitation upon electron detachment. The HOMO−1 is also mainly of the π^* of O_2 (Figure 3h). These frontier orbitals are characteristic of the superoxo chemisorption state in the $O_2Au_n^-$ complexes for n = 2, 4, 6, and 20, whose PES spectra all contain broad low binding energy features derived from the π^* orbitals of O_2^- (Figure 1). Very importantly, the HOMO of the peroxo isomer of $O_2Au_8^-$ (Figure 3e) is mainly from the Au_8-backbone. The HOMO−1 of the peroxo isomer (Figure 3f) also has contributions from the Au-backbone. These orbitals are similar to those for the peroxo isomer of $O_2Au_6^-$ (Figure 3c,d). It is expected that electron detachment from these Au-based orbitals would result in relatively sharp PES bands. Thus, both the simulated PES spectral patterns and the nature of the frontier orbitals for the two molecularly chemisorbed isomers are consistent with the experimental observation for $O_2Au_8^-$.

The bare Au_8^- cluster is known to have two nearly degenerate planar global minimum structures[39] with D_{4h} and C_{2v} symmetries, respectively. The current study shows that O_2 reacts with the D_{4h} isomer to form the superoxo state, whereas it reacts with the C_{2v} isomer to form the peroxo $O_2Au_8^-$. Our previous O_2 titration experiment showed that the C_{2v} isomer is more reactive toward O_2,[39] consistent with the current conclusion that the peroxo $O_2Au_8^-$ is more stable than the superoxo state. The superoxo $O_2Au_8^-$ can be viewed as a one-electron transfer from Au_8^- to O_2 to form the superoxo O_2^- on the Au_8 surface. This mechanism was first suggested by Salisbury et al.[20] and should be operational for the reaction of O_2 with Au_2^-, Au_4^-, Au_6^-, and Au_{20}^-. All these anions have very low electron binding energies or the corresponding neutrals have very low electron affinities and large HOMO−LUMO gaps. Indeed, the D_{4h} isomer of Au_8^- has a slightly lower electron binding energy than the C_{2v} isomer and the corresponding neutral Au_8 has very larger HOMO−LUMO gap,[35] consistent with the electron transfer mechanism.

The PES data shown in Figure 2c and 2d suggests that the superoxo $O_2Au_8^-$ can be transformed to the more stable peroxo chemisorption state at longer reaction time, i.e. for $O_2Au_8^-$ the superoxo chemisorption state is a kinetically controlled product. We have located the transition state and calculated the barrier for the superoxo to peroxo conversion, as shown in Figure 4. The 0.434 eV barrier height should be accessible

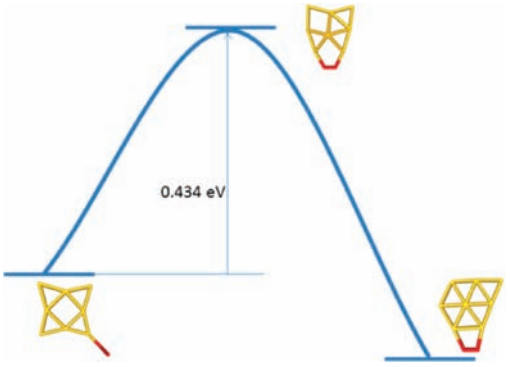

Figure 4. The reaction path for the conversion from the superoxo to peroxo isomer of $O_2Au_8^-$. The O−O bond length in the superoxo isomer (where one O atom is bonded to gold) is 1.28 Å and it is 1.30 Å in the peroxo isomer (where both O atoms are bonded to gold).

under our experimental conditions at room temperature. It is important to note that the O−O distance in the superoxo state is 1.28 Å, whereas in the peroxo state it is 1.30 Å. The elongation of the O−O bond in the peroxo state suggests that O_2 is more activated in the peroxo state, which would be important for the subsequent reaction with CO to form CO_2, for example.

In order to differentiate the two molecular chemisorption structures of $O_2Au_8^-$, we have computed the electron spin densities on every atom for both the peroxo and superoxo isomers, as shown in Table 4. The O1 and O2 label in the superoxo state represent the oxygen atoms unbound and bonded to the Au_8 cluster, respectively. The spin densities of the O1 and O2 atoms in the superoxo state are very different; whereas in the peroxo state they are much closer in value. The combined spin densities of the two O atoms are slightly higher for the superoxo species than the peroxo species, indicating a slightly higher magnetic moment for the O_2 unit in the superoxo structure than in the peroxo structure. In other words, the magnetic moment of O_2 in the superoxo isomer is closer to that of the gas-phase O_2, hence the O_2 is less activated compared to the peroxo state.

Table 4. Calculated Spin Densities on Every Atoms of the Superoxo [Isomer (c)] and Peroxo [Isomer (b)] Forms of $O_2Au_8^-$

isomer (b) (peroxo)	spin densities	isomer (c) (superoxo)	spin densities
O1	0.415	**O1**	0.751
O2	0.543	**O2**	0.278
Au3	−0.004	**Au3**	−0.014
Au4	−0.011	**Au4**	−0.011
Au5	−0.002	**Au5**	0.002
Au6	0.005	**Au6**	0.0001
Au7	0.028	**Au7**	0.002
Au8	0.026	**Au8**	−0.0001
Au9	−0.017	**Au9**	−0.011
Au10	0.017	**Au10**	0.004

We further computed the projected density of states (PDOS) of O_2 on the two molecularly chemisorbed $O_2Au_8^-$ isomers (Figure 5b,c), compared to that of gas-phase O_2 (Figure 5a). The blue and red lines in Figure 5 represent the α and β PDOS. Note that the two unpaired electrons in molecular O_2 are assigned to the α spin-state by convention. Each sharp band is

dx.doi.org/10.1021/ja302902p | J. Am. Chem. Soc. 2012, 134, 9438−9445

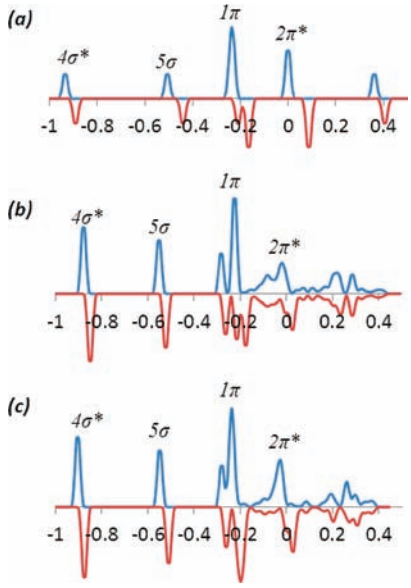

Figure 5. The PDOS of (a) free O_2, (b) peroxo $O_2Au_8^-$, and (c) superoxo $O_2Au_8^-$. The unit of the orbital energies in the *x*-axis is hartree.

indicative of an electronic state (e.g, $4\sigma^*$, 5σ, 1π, etc.). The α and β PDOS cannot exactly overlap with each other, indicating a net magnetic moment for both gas-phase and the chemisorbed species. In the $O_2Au_8^-$ complex, certain electrons of the Au-cluster is transferred to the π^* orbital of O_2 and as a result, the net spin is lowered, which gives rise to a much closer gap between the α and β PDOS than in gas-phase O_2. However near the Fermi level (0 in the *x*-axis in Figure 5) the $\alpha-\beta$ gap of the $2\pi^*$ state for the peroxo species is slightly less than that for the superoxo species. This feature suggests that the superoxo species entails slightly higher magnetic moment (due to less charge transfer from Au_8^-) than the peroxo species. Hence, the molecular O_2 in the peroxo state is slightly more activated and possesses a slightly longer bond length.

The observation and confirmation of the two molecular chemisorption states of O_2 on Au_8^- is significant. Because all molecular O_2 adsorption observed for smaller anions $O_2Au_n^-$ (n = 2, 4, 6) were shown to be the superoxo type, Au_8^- is then the critical size for the transition from superoxo to peroxo chemisorption for O_2 activation with the exception of Au_{20}^-, which has an extremely low electron binding energy and a unique high symmetry tetrahedral structure.[44] Theoretical calculations also suggest that O_2 chemisorbs on the tetrahedral Au_{20}^- in the superoxo state.[45] The lack of the superoxo-derived features in the PES spectra of $O_2Au_{12}^-$, $O_2Au_{14}^-$, and $O_2Au_{18}^-$ (Figure 1) suggests O_2 is likely in the peroxo state in these clusters, as shown below.

$O_2Au_{12}^-$. It is known that for the bare anionic gold clusters, the 2D-to-3D transition occurs at Au_{12}^- where the 2D planar isomer exhibits D_{3h} symmetry while the 3D isomer exhibits C_{2v} symmetry.[46,47] For $O_2Au_{12}^-$, our basin-hopping search combined with DFT optimization generated about 800 structures, consisting of both molecularly chemisorbed and dissociated isomers. The lowest-energy dissociated isomer and the top candidate chemisorbed structures were reevaluated at the SO-PBE0/CRENBL level of calculations and the computed photoelectron spectra along with relative energies are presented in Figure S4 (SI). Indeed, the lowest-energy chemisorbed $O_2Au_{12}^-$, which is in the peroxo state (with O−O bond length 1.33 Å), gives the best agreement with the experimental PES spectrum (Figure 2f,g). Moreover, the HOMO and HOMO−1 of the peroxo isomer of $O_2Au_{12}^-$ (Figure S5 (SI)) are mainly from the Au_{12}-backbone, similar to those for the peroxo isomer of $O_2Au_8^-$. As expected, the electron detachment from these Au-based orbitals results in relatively sharp PES bands. In summary, both the simulated PES spectral patterns and the nature of the frontier orbitals for the molecularly chemisorbed isomer are consistent with the experimental observation for $O_2Au_{12}^-$.

$O_2Au_{14}^-$. For $O_2Au_{14}^-$, our basin-hopping search combined with DFT optimization generated about 1000 structures, consisting of both molecularly chemisorbed and dissociated isomers. Again, the lowest-energy dissociated isomer and the top candidate chemisorbed structures were reevaluated using SO-PBE0/CRENBL calculations, and the computed photoelectron spectra along with relative energies are presented in Figure S6 (SI). Indeed, the lowest-energy chemisorbed $O_2Au_{14}^-$, which is in the peroxo state (with O−O bond length 1.32 Å), gives the best agreement with the experimental PES spectrum (Figure 2h,i). Moreover, the HOMO and HOMO−1 of the peroxo isomer of $O_2Au_{14}^-$ (Figure S7 (SI)) are mainly from the Au_{14}-backbone, similar to those for the peroxo isomer of $O_2Au_8^-$ and $O_2Au_{12}^-$. Likewise, the electron detachment from these Au-based orbitals results in relatively sharp PES bands. Again, both the simulated PES spectral patterns and the nature of the frontier orbitals for the molecularly chemisorbed isomer are consistent with the experimental observation for $O_2Au_{14}^-$.

$O_2Au_{18}^-$. The bare Au_{18}^- is known to exist in both cage and pyramidal forms in the cluster beam.[48] In our previous study[48] we showed that the relative population of the cage and pyramid isomers can be altered by using a small amount (0.1%) of O_2 seeded in the helium carrier gas. The cage isomer was found to be more reactive with O_2 than the pyramidal isomer and therefore can be "preferentially titrated" from the cluster beam. In the present study our observation indicates again that the cage isomer is the dominant species in the cluster beam of $O_2Au_{18}^-$. The experimental photoelectron spectrum of $O_2Au_{18}^-$ (Figure 2j) shows congested peaks in the region of 4.3—5.3 eV. Our basin-hopping global minimum search generated nearly 600 consistent sets of low-energy isomers. Figure S8 (SI) shows the computed PES spectra of several low-lying isomers along with their relative energies at both SO-PBE0/CRENBLE and TPSSh levels of theory. Nearly all the structures possess either cage or pyramidal Au_{18}^- structures with peroxo or superoxo chemisorption of O_2. Isomer (a) is the lowest in energy at the SO-PBE0 level and represents the cage-like Au_{18}^- with the peroxo O_2 chemisorption (Figure S8a [SI]). In contrast, the pyramidal isomer (b) with the peroxo O_2 binding is the lowest-lying isomer at the TPSSh level. The simulated spectrum of isomer (a) is in good agreement with the experimental spectrum (Figure 2k). The computed spectrum of isomer (b) shows a rather low first VDE (3.71 eV) and a gap of about 0.4 eV between the first and second VDE. These features are clearly not in agreement with the experimental spectrum, suggesting that isomer (b) should be much higher in energy than the cage isomer (a) and was not present in the cluster beam in any significant amount. The HOMO and HOMO−1 of isomer (a) are shown in Figure S9 (SI). The HOMO is largely from the Au backbone; the HOMO−1 has slight contributions from the O−O π^* orbital. The nature of the

dx.doi.org/10.1021/ja302902p | J. Am. Chem. Soc. 2012, 134, 9438−9445

HOMO in the peroxo isomer is consistent with the high VDEs observed experimentally for $O_2Au_{18}^-$.

CONCLUSION

In conclusion, we have found that there exist two modes of O_2 chemisorption onto even-sized Au_n^- clusters: the superoxo and peroxo states. For the clusters with very low electron binding energies (n = 2, 4, 6, 20) or large HOMO−LUMO gaps in the corresponding neutral clusters, O_2 is chemisorbed in the superoxo form via one electron charge transfer from Au_n^- to O_2. We find that Au_8^- is the onset for the superoxo to peroxo chemisorption. In the peroxo form, both O atoms interact with the underlying Au_n^- clusters and the O−O bond is more activated, i.e., more elongated than that in the superoxo form. Hence, the Au_8^- cluster is the smallest anionic gold nanoparticle that entails peroxo binding with O_2. Considering the fact that in the peroxo state O_2 is much more activated, the current observation suggests that this mode of chemisorption may play a more prominent role in the O_2 activation by gold nanoparticles and provides a key insight in elucidating the catalytic mechanisms of nanogold.

ASSOCIATED CONTENT

Supporting Information

Isomer structures, energies, simulated photoelectron spectra for $O_2Au_n^-$ (n = 6, 8, 12, 14, 18), and HOMO and HOMO−1 pictures for n = 12, 14, 18; dissociation pathways and activation barrier for $O_2Au_8^-$; and vibrational frequencies for the top 14 isomers of $O_2Au_8^-$. This material is available free of charge via the Internet at http://pubs.acs.org.

AUTHOR INFORMATION

Corresponding Author

lai-sheng_wang@brown.edu (L.-S.W.); xzeng1@unl.edu (X.C.Z.)

Notes

The authors declare no competing financial interest.

Note Added in Review. During the review of this manuscript, Woodham et al.[49] published a paper on an infrared spectroscopy study of chemisorption of molecular O_2 on Au_4^-−Au_{10}^-. We note that the lowest-energy isomer of $O_2Au_6^-$ and the two lowest-lying isomers of $O_2Au_8^-$ reported in ref 49 are similar to the results in the present work.

ACKNOWLEDGMENTS

The experimental work was supported by the National Science Foundation (CHE-1049717 to L.S.W.). The theoretical work at UNL was supported by grants from the NSF (EPS-1010674) and ARL (W911NF1020099) and by University of Nebraska's Holland Computing Center. Y.P. is partially supported by the Academic Leader Program in Xiangtan University (10QDZ34) and Natural Science Foundation of China (Grant No. 21103144).

REFERENCES

(1) Haruta, M. *Catal. Today* **1997**, *36*, 153.
(2) Nijhuis, T. A.; Visser, T.; Weckhuysen, B. M. *J. Phys. Chem. B.* **2005**, *109*, 19309.
(3) Sinha, A. K.; Seelan, S.; Tsubota, S.; Haruta, M. *Top. Catal.* **2004**, *29*, 95.
(4) McEwan, L.; Julius, M.; Roberts, S.; Fletcher, J. C. Q. *Gold Bull. (London, U.K.)* **2010**, *43* (4), 298.
(5) Tsunoyama, H.; Sakurai, H.; Ichikuni, N.; Negishi, Y.; Tsukuda, T. *Langmuir* **2004**, *20*, 11293.
(6) Bond, G. C. *Gold Bull. (London, U.K.)* **2009**, *42*, 337.
(7) Haruta, M.; Tsubota, S.; Kobayashi, T.; Kageyama, H.; Genet, M. J.; Delmon, B. *J. Catal.* **1993**, *144*, 175.
(8) Wallace, W. T.; Whetten, R. L. *J. Phys. Chem. B* **2000**, *104*, 10964.
(9) Wallace, W. T.; Whetten, R. L. *J. Am. Chem. Soc.* **2002**, *124*, 7499.
(10) Burgel, C.; Reilly, N. M.; Johnson, G. E.; Mitric, R.; Kimble, M. L.; Castleman, A. W., Jr.; Bonačić-Koutecký, V. *J. Am. Chem. Soc.* **2008**, *130*, 1694.
(11) Valden, M.; Lai, X.; Goodman, D. W. *Science* **1998**, *281*, 1647.
(12) Lopez, N.; Norskov, J. K. *J. Am. Chem. Soc.* **2002**, *124*, 11262.
(13) Socaciu, L. D.; Hagen, J.; Bernhardt, T. M.; Wöste, L.; Heiz, U.; Häkkinen, H.; Landman, U. *J. Am. Chem. Soc.* **2003**, *125*, 10437.
(14) Neumaier, M.; Weigend, F.; Hampe, O.; Kappes, M. *J. Chem. Phys.* **2005**, *122*, 104702.
(15) Lemire, C.; Meyer, R.; Shaikhutdinov, S.; Freund, H. J. *Angew. Chem., Int. Ed.* **2004**, *43*, 118.
(16) Yoon, B.; Hakkinen, H.; Landman, U.; Wirz, A. S.; Antonietti, J. M.; Abbet, S.; Heiz, U. *Science* **2005**, *307*, 403.
(17) Häkkinen, H.; Landman, U. *J. Am. Chem. Soc.* **2001**, *123*, 9704.
(18) Cox, D. M.; Brickman, R. O.; Greegan, K.; Kaldor, A. Z. *Z. Phys. D: At., Mol. Clusters* **1991**, *19*, 353.
(19) Lee, T. H.; Ervin, K. M. *J. Phys. Chem.* **1994**, *98*, 10023.
(20) Salisbury, B. E.; Wallace, W. T.; Whetten, R. L. *Chem. Phys.* **2000**, *262*, 131.
(21) Stolcic, D.; Fischer, M.; Gantefor, G.; Kim, Y. D.; Sun, Q.; Jena, P. *J. Am. Chem. Soc.* **2003**, *125*, 2848.
(22) Kim, Y. D.; Fischer, M.; Gantefor, G. *Chem. Phys. Lett.* **2003**, *377*, 170.
(23) Huang, W.; Zhai, H. J.; Wang, L. S. *J. Am. Chem. Soc.* **2010**, *132*, 4344.
(24) Bulusu, S.; Li, X.; Wang, L. S.; Zeng, X. C. *Proc. Natl. Acad. Sci. U.S.A.* **2006**, *103*, 8326.
(25) Huang, W.; Wang, L. S. *Phys. Chem. Chem. Phys.* **2009**, *11*, 2663.
(26) Yoon, B.; Häkkinen, H.; Landman, U. *J. Phys. Chem. A* **2003**, *107*, 4066.
(27) Sun, Q.; Jena, P.; Kim, Y. D.; Fischer, M.; Gantefor, G. *J. Chem. Phys.* **2004**, *120*, 6510.
(28) Varganov, S. A.; Olson, R. M.; Gordon, M. S.; Metiu, H. *J. Chem. Phys.* **2003**, *119*, 2531.
(29) Mills, G.; Gordon, M. S.; Metiu, H. *Chem. Phys. Lett.* **2002**, *359*, 493.
(30) Ding, X.; Li, Z.; Yang, J. L.; Hou, J. G.; Zhu, Q. *J. Chem. Phys.* **2004**, *120*, 9594.
(31) Ding, X.; Dai, B.; Yang, J. L.; Hou, J. G.; Zhu, Q. *J. Chem. Phys.* **2004**, *121*, 621.
(32) Wang, Y.; Gong, X. G. *J. Chem. Phys.* **2004**, *125*, 124703.
(33) Boronat, M.; Corma, A. *Dalton. Trans.* **2010**, *39*, 8538.
(34) Lyalin, A.; Taketsugu, T. *J. Phys. Chem. Lett.* **2010**, *1*, 1752.
(35) Wang, L. S.; Cheng, H. S.; Fan, J. *J. Chem. Phys.* **1995**, *102*, 9480.
(36) Wales, D. J.; Scheraga, H. A. *Science* **1999**, *285*, 1368.
(37) Yoo, S.; Zeng, X. C. *J. Chem. Phys.* **2003**, *119*, 1442.
(38) Bylaska, E. J.; DeJong, W. A.; Govind, N.; Kowalski, K.; Straatsma, T. P.; Valiev, M.; Wang, D.; Apra, E.; Windus, T. L.; Hammond, J.; Nichols, P.; Hirata, S.; Hackler, M. T.; Zhao, T.; Fan, P. D.; Harrison, T. J.; Dupuis, M.; Smith, D. M. A.; Nieplocha, J.; Tipparaju, V.; Krishnan, M.; Wu, Q.; Van Voorhis, T.; Auer, A. A.; Nooijen, M.; Brown, E.; Cisneros, G.; Fann, G. I.; Fruchtl, H.; Garza, J.; Hirao, K.; Kendall, R.; Nichols, J. A.; Tsemekhman, K.; Wolinski, K.; Anchell, J.; Bernholdt, D.; Borowski, P.; Clark, T.; Clerc, D.; Dachsel, H.; Deegan, M.; Dyall, K.; Elwood, D.; Glendening, E.; Gutowski, M.; Hess, A.; Jaffe, J.; Johnson, B.; Ju, J.; Kobayashi, R.; Kutteh, R.; Lin, Z.; Littlefield, R.; Long, X.; Meng, B.; Nakajima, T.; Niu, S.; Pollack, L.; Rosing, M.; Sandrone, G.; Stave, M.; Taylor, H.; Thomas, G.; Van Lenthe, J., Wong, A.; Zhang, Z. *NWCHEM*, a computational chemistry package for parallel computers, version 5.1.1; Pacific Northwest National Laboratory: Richland, WA, 2010.

(39) Huang, W.; Pal, R.; Wang, L.-M.; Zeng, X. C.; Wang, L. S. *J. Chem. Phys.* **2010**, *132*, 054305.
(40) Wang, L.-M.; Pal, R.; Huang, W.; Zeng, X. C.; Wang, L. S. *J. Chem. Phys.* **2010**, *132*, 114306.
(41) Pal, R.; Wang, L.-M.; Huang, W.; Wang, L. S.; Zeng, X. C. *J. Chem. Phys.* **2011**, *134*, 054306.
(42) Shao, N.; Huang, W.; Gao, Y.; Wang, L.-M.; Li, X.; Wang, L. S.; Zeng, X. C. *J. Am. Chem. Soc.* **2010**, *132*, 6596.
(43) Pal, R.; Huang, W.; Wang, Y. L.; Hu, H. S.; Bulusu, S.; Xiong, X. G.; Li, J.; Wang, L. S.; Zeng, X. C. *J. Phys. Chem. Lett.* **2011**, *2*, 2288.
(44) Li, J.; Li, X.; Zhai, H. J.; Wang, L. S. *Science* **2003**, *299*, 864.
(45) Molina, L. M.; Hammer, B. *J. Catal.* **2005**, *233*, 399.
(46) Furche, F.; Ahlrichs, R.; Weis, P.; Jacob, C.; Gilb, S.; Bierweiler, T.; Kappes, M. M. *J. Chem. Phys.* **2002**, *117*, 6982.
(47) Huang, W.; Wang, L.-S. *Phys. Rev. Lett.* **2009**, *102*, 153401.
(48) Huang, W.; Bulusu, S.; Pal, R.; Zeng, X. C.; Wang, L. S. *ACS Nano* **2009**, *3*, 1225.
(49) Woodham, A. P.; Meijer, G.; Feilicke, A. *Angew. Chem., Int. Ed.* **2012**, *51*, 4444.